IEEE Access
Multidisciplinary | Rapid Review | Open Access Journal

Date of publication xxxx 00, 0000, date of current version xxxx 00, 0000.

Digital Object Identifier 10.1109/ACCESS.2019.Doi Number

Robust Direction-of-Arrival Estimation for Coprime Array in the Presence of Miscalibrated Sensors

JIAXUN KOU, MING LI, AND CHUNLAN JIANG,
State Key Laboratory of Explosion Science and Technology, Beijing Institute of Technology, Beijing 100081, China

Corresponding author: Chunlan Jiang (e-mail: jiangchunwh@bit.edu.cn).

This work was supported in part by the National Natural Science Foundation under Grant 11672042.

ABSTRACT Coprime arrays have been widely adopted for direction-of-arrival (DOA) estimation since it can achieve an increased number of degrees of freedom (DOF). To utilize all information received by the coprime array, array interpolation methods are developed, which construct a virtual uniform linear array (ULA) with the same aperture from the non-uniform coprime array. However, the conventional non-robust DOA estimation algorithms for coprime arrays, including the interpolation based methods, suffer from degraded performance or even failed operation when some sensors are miscalibrated. In this paper, a novel maximum correntropy criterion (MCC) based virtual array interpolation algorithm for robust DOA estimation is developed to address this problem. The proposed approach treats the miscalibrated sensor observations as outliers, and by exploiting the property of MCC, the interpolated virtual array covariance matrix is reconstructed via nuclear norm minimization (NNM) with less influence of these outliers. In this manner, the robust DOA estimation is enabled by the robustly reconstructed covariance matrix. Simulation results demonstrate that the proposed algorithm can effectively the mitigate effect of the miscalibrated sensors while maintaining the enhanced DOF offered by coprime arrays.

INDEX TERMS Coprime array, calibration error, virtual array interpolation, maximum correntropy criterion (MCC), robust direction-of-arrival (DOA) estimation.

I. INTRODUCTION

Direction-of-arrival (DOA) estimation of energy-emitting sources is one of fundamental array signal processing technique which finds broad applications in radar, sonar, acoustic, navigation and wireless communication [1-3]. On the basis of the Nyquist sampling constraint, the uniform linear array (ULA) is the mostly adopted configuration. Nevertheless, using ULAs, classical DOA estimation algorithms can only resolve up to $M-1$ sources with M sensors [4, 5]. Recently, sparse linear arrays, such as coprime arrays and nested arrays, received considerable attentions duo to their abilities to break through this limitation. For instance, the coprime arrays can be used to resolve $\mathcal{O}(MN)$ sources with only $M+N-1$ physical sensors [6].

To exploit the enhanced degree of freedom (DOF) offered by coprime array, a preprocessing procedure is taken, which derives an augmented virtual array by computing the difference coarray. And then the corresponding virtual array signals are implemented for DOA retrieval [7]. Since the covariance matrix obtained from the virtual array signals is rank one, decorrelation operation has to be applied to restore the full matrix rank [8]. The most popular decorrelation method is the spatial smooth technique, which requires a ULA based signal model. Because the coprime array is partly augmented, there are holes in its derived coarray [9]. A common scheme is to extract the continuous segment for the spatial smooth processing, and then implement the subspace-based DOA estimation algorithm, MUltiple Signals Classification (MUSIC). Thus, the SS-MUSIC (spatial smooth MUSIC) algorithm is yield. Apparently, the SS-MUSIC algorithm suffers from performance loss since it discards the discontinuous virtual array sensors. Although compressive sensing (CS) based DOA estimation methods use entire information received by the array, they require discretization of parameter space into a dense grid which leads to high computational cost. In addition, they do not work well for off grid targets [6]. A different gridless approach to include full coarray information is to fill the

holes by interpolating the missing samples. Based on nuclear norm minimization (NNM), an interpolation algorithm for DOA estimation is proposed in [6], which reconstructs a low rank Toeplitz covariance matrix of signals received at the physical array. Similarly, the algorithms proposed in [10] and [11] interpolating the missing samples by minimizing the atomic norm of the second-order virtual signals.

The excellent performance of abovementioned coarray based DOA estimation is depended heavily on the assumption that all sensors in the physical array are properly calibrated [12]. However, it is difficult to avoid the sensor error completely in practice, leading to degraded performance or even estimation failure. To address this problem, a lot of calibration methods or robust DOA estimation methods have been developed. Among them, the self-calibration methods jointly estimate the DOAs of signals and array error parameters under the assumption that the array calibration errors can be modeled as deterministic unknown quantities. For instances, several self-calibration methods [13-15] are developed based on the eigenstructure of signal covariance matrix. Nevertheless, these eigenstructure based methods exploit the orthogonality property between the signal subspace and noise subspace, so they cannot be applied for the coprime array with the expectation to find more sources than sensors. Based on compressive sensing, Liu *et al.* propose another joint estimation method, named Sparse Bayesian Array Calibration (SBAC), for array calibration [16] under the sparse Bayesian learning (SBL) framework. In [17], the SBAC method is applied for sparse array calibration with second order virtual signal model. The enhanced DOF offered by the sparse array can be exploited by the SBAC method, however it is computationally intensive and it works well only when the array perturbation is small. Except for the self-calibration methods, other robust methods that do not explicitly estimate the error parameters are also proposed for DOA estimation in the presence of miscalibrated sensors. With the assumption that few sensors in the sensor array are miscalibrated, Wang *et al.* introduced a CS based robust DOA estimation method in [18], which treats miscalibrated sensor observations as outliers and employs the maximum correntropy criterion (MCC) as a constraint function to suppress the influence of outliers while fusing the data observed at different sensors. In one of our previously published paper [19], we applied this MCC incorporated CS based DOA estimation method for the coprime array; meanwhile a grid refinement strategy is developed to alleviate the grid mismatch problem.

In this paper, a novel interpolation based robust DOA estimation method is proposed for coprime array in the presence of miscalibrated sensors. Under the same assumption as in [18] about the miscalibrated sensors, we first model the interpolation process as a nuclear norm minimization (NNM) problem of the virtual signals belonging to the second-order statistics. Different from the NNM based methods in [6] and [8], the MCC is employed in our established NNM model as the constraint to suppress the perturbations caused by the outliers. Since the MCC embedded NNM problem is non-convex, an iterative algorithm, referred to as IMCC-NNM, is then derived to effectively solve it. After the convergence of the IMCC-NNM, the subspace based DOA estimation method, such as MUSIC, can be directly used with the reconstructed covariance matrix. Thus, the robust DOA estimation is enabled with the enhanced DOF in a gridless manner. Simulation results demonstrate the superiorities of the proposed IMCC-NNM algorithm in terms of the robustness.

The main contributions of this paper can be summarized as follow:

- We introduce the MCC into the NNM based interpolation process, by using which the influence of the outliers can be effectively mitigated without *a priori* knowledge about the sensor miscalibrations.
- We develop an iterative algorithm to effectively solve the optimization problem arising in the MCC embedded interpolation process and prove its convergence
- We robustly reconstruct a Hermitian Toeplitz covariance matrix with all coarray information in a gridless manner, and provide the theoretical performance analyses.

The rest of this paper is organized as follow. In Section II, the signal model of the coprime array with miscalibrated sensors is given. The theories of NNM interpolation method and MCC are reviewed in Section III. Then a robust virtual array interpolation based DOA estimator is proposed in Section IV for coprime array in the presence of miscalibrated sensors, where some performance analyses also presented. In Section V, a series of simulations are presented. Finally, some concluding remarks are drawn in Section VI.

Notations: Throughout this paper, the lower-case boldface characters, upper-case boldface characters, and upper-case characters in blackboard boldface are used to denote vectors, matrices, and sets respectively. $\mathbb{C}^{M\times N}$ denotes a complex matrix or vector (when $N = 1$). The superscripts $(\cdot)^{\mathrm{T}}$, $(\cdot)^{\mathrm{H}}$ and $(\cdot)^{*}$ denote the transpose, conjugate transpose, and complex conjugation, respectively. $(\cdot)^{-1}$ and $\mathbf{tr}(\cdot)$ respectively denote the inverse and the trace of a matrix. $[\mathbf{A}]_{i,j}$ indicates the (i, j)-th entry of a matrix $\mathbf{A}$. The square bracket notation of a vector $[\mathbf{x}_{\mathbb{S}}]_i$ represents the i-th component of $\mathbf{x}_{\mathbb{S}}$. For $n \in \mathbb{S}$, the triangular bracket notation $\langle \mathbf{x}_{\mathbb{S}} \rangle_n$ denotes the signal value at the support location n, where the detailed definition is given in [7]. The notation $\mathrm{E}[\cdot]$ denotes the statistical expectation. $\mathrm{vec}(\cdot)$ stands for the vectorization operator that sequentially stacks each column of a matrix, and $\mathrm{diag}(\cdot)$ represents a diagonal matrix with the corresponding elements on its diagonal. The symbols $\circ$, $\odot$

This article has been accepted for publication in a future issue of this journal, but has not been fully edited. Content may change prior to final publication. Citation information: DOI 10.1109/ACCESS.2020.2971842, IEEE Access

and $\otimes$ represent the Hadamard product, Khatri-Rao product and Kronecker product respectively. $\mathbf{I}$ denotes the identity matrix with an appropriate dimension. Finally, the symbol j represents imaginary unit $\sqrt{-1}$.

II. PROBLEM FORMULATION

A. SIGNAL MODEL OF COPRIME ARRAY

In this work, the extended coprime array is employed, which is generated by the coprime integers pair $\{M, N\}$. An extended coprime array can be viewed as the union of two sparsely spaced uniform linear sub-arrays, and without loss of generality, assume that $M < N$. Then, as shown in Fig. 1, one of the subarrays consisting of $2M$ sensors has an inter-element spacing of Nd, whereas the other one with N sensors has an inter-element spacing of Md. Here, the unit spacing d is a half-wavelength, i.e., $d = \lambda/2$. Therefore, the coprime array contains $|\mathbb{S}| = 2M + N - 1$ physical sensors, which have locations $\mathbb{L} = \{l_1, l_2, ..., l_{2M+N-1}\} = \mathbb{S} \times d$, where $\mathbb{S}$ is an integer set given by

$$\mathbb{S} = \{Mn \mid 0 \le n \le N-1\} \bigcup \{Nm \mid 0 \le m \le 2M-1\}, \quad (1)$$

and $|\cdot|$ denotes the cardinality of a set. Moreover, the aperture of the coprime array is $(2M-1)Nd$.

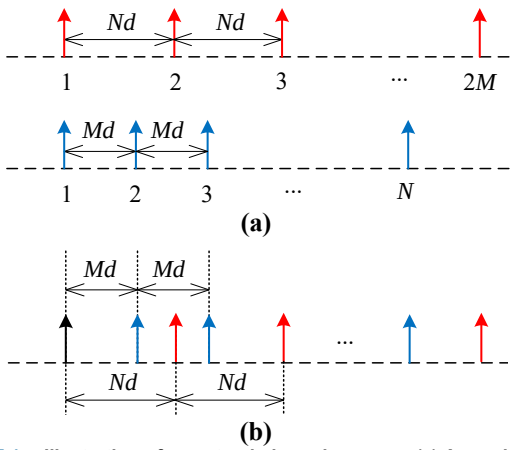

FIGURE 1. Illustration of an extended coprime array. (a) A coprime pair of sparse ULAs. (b) Coprime array configuration.

Assuming K uncorrelated far-field narrowband sources impinging on the coprime array from directions $\boldsymbol{\theta} = [\theta_1, \theta_2, ..., \theta_K]^{\mathrm{T}}$, the T snapshots received by the array can be modeled as

$$\mathbf{x}(t) = \sum_{k=1}^{K} \mathbf{a}(\theta_k) s_k(t) + \mathbf{n}(t) = \mathbf{A}\mathbf{s}(t) + \mathbf{n}(t) \quad t = 1, 2, ..., T, \quad (2)$$

where $\mathbf{A} = [\mathbf{a}(\theta_1), \mathbf{a}(\theta_2), ..., \mathbf{a}(\theta_K)] \in \mathbb{C}^{(2M+N-1)\times K}$ is the coprime array steering matrix (or manifold matrix) with k-th column,

$$\mathbf{a}(\theta_k) = \left[1, e^{-j\frac{2\pi}{\lambda} l_2 \sin(\theta_k)}, ..., e^{-j\frac{2\pi}{\lambda} l_{|\mathbb{S}|} \sin(\theta_k)}\right]^{\mathrm{T}} \quad (3)$$

representing the steering vector of the k-th source, $\mathbf{s}(t) = [s_1(t), s_2(t), ..., s_K(t)]^{\mathrm{T}}$ denotes the source signal vector, and $\mathbf{n}(t) \sim \mathcal{CN}(\mathbf{0}, \sigma_n^2 \mathbf{I})$ represents the independent and identical distributed (i.i.d) zero-mean addictive white Gaussian noise vector, and σ_n^2 denotes the noise power.

The covariance matrix of the array output $\mathbf{x}(t)$ is

$$\mathbf{R}_{\mathbb{S}} = \mathrm{E}\left[\mathbf{x}(t)\mathbf{x}^{\mathrm{H}}(t)\right] = \sum_{k=1}^{K} p_k \mathbf{a}(\theta_k)\mathbf{a}^H(\theta_k) + \sigma_n^2 \mathbf{I}, \quad (4)$$

where p_k denotes the power of k-th source. Because of the fact that the theoretical $\mathbf{R}_{\mathbb{S}}$ is unavailable, it is usually replaced by its maximum likelihood (ML) estimation

$$\hat{\mathbf{R}}_{\mathbb{S}} = \frac{1}{T} \sum_{t=1}^{T} \mathbf{x}(t)\mathbf{x}^{\mathrm{H}}(t), \quad (5)$$

and $\hat{\mathbf{R}}_{\mathbb{S}}$ will converge to $\mathbf{R}_{\mathbb{S}}$ as $T \to \infty$ under the stationary and ergodicity assumption [20].

B. EFFECT OF MISCALBRATED SENSORS

When there exists some miscalibrated sensors in the array, the observations received by them are affected by unknown gain and phase distortions. In this work, these distorted observations are treated as outliers of the array outputs. Denote $\mathbb{M}$ as the set of miscalibrated sensors, and assume that the number of miscalibrated sensors, M_d, is less than the number of sensors in the coprime array, i.e. $M_d = |\mathbb{M}| < (2M + N - 1)$. If the m-th array sensor is miscalibrated, the distorted signals received from it can be modeled as

$$x_m^o(t) = \sum_{k=1}^{K} \gamma_m a_m(\theta_k) s_k(t) + n_m(t). \quad (6)$$

where $\gamma_m = \rho_m e^{j\phi_m}$ is an unknown complex factor, while ρ_m and ϕ_m stands for gain distortion and phase distortion respectively; $a_m(\theta_k)$ denotes the m-th entry of $\mathbf{a}(\theta_k)$.

In this manner, the received snapshots in (2) are rewritten as

$$\mathbf{x}^o(t) = \boldsymbol{\Gamma}\mathbf{A}\mathbf{s}(t) + \mathbf{n}(t), \quad (7)$$

where $\boldsymbol{\Gamma}$ is a diagonal matrix, in which the m-th diagonal entry can be expressed as

$$\Gamma_{m,m} = \gamma_m = \begin{cases} \rho_m e^{j\phi_m}, & m \in \mathbb{M} \\ 1, & m \notin \mathbb{M} \end{cases}. \quad (8)$$

As shown in (7), in the presence of miscalibrated sensors, the actual manifold matrix becomes $\boldsymbol{\Gamma}\mathbf{A}$, which is different from the assumed original manifold matrix $\mathbf{A}$. As a result, the DOA methods based on the unperturbed steering manifold will suffer from inaccuracy or even failure. Therefore, the objective of this paper is to mitigate the influence of the sensor miscalibrations and improve the DOA estimation accuracy without explicitly estimating gain-phase errors (ρ_m and ϕ_m). Meanwhile, the covariance matrix is distorted into $\mathbf{R}_{\mathbb{S}}^o$, which is expressed by

$$\mathbf{R}_{\mathbb{S}}^{o}=\mathbf{\Gamma}\mathbf{A}\mathbf{s}(t)\mathbf{s}(t)^{\mathrm{H}}\mathbf{A}^{\mathrm{H}}\mathbf{\Gamma}^{\mathrm{H}}+\sigma_n^2\mathbf{I}. \tag{9}$$

In practice, it is calculated as

$$\hat{\mathbf{R}}_{\mathbb{S}}^{o}=\left(1/T\right)\sum_{t=1}^{T}\mathbf{x}^{o}(t)\left(\mathbf{x}^{o}(t)\right)^{\mathrm{H}}. \tag{10}$$

III. RELATED WORKS

A. COARRAY INTERPOLATION VIA NNM

With a coprime array, the increased number of DOF is achieved by operating the derived equivalent virtual signals. In distortionless cases, vectorizing the covariance matrix, the virtual array signals are obtained as

$$\mathbf{x}_{\mathbb{D}}=\mathrm{vec}(\mathbf{R}_{\mathbb{S}})=\mathbf{A}_{\mathbb{D}}\mathbf{p}+\sigma_n^2\mathbf{i}, \tag{11}$$

where $\mathbf{A}_{\mathbb{D}}=\mathbf{A}^{*}\odot\mathbf{A}\in\mathbb{C}^{(2M+N-1)^2\times K}$, $\mathbf{p}=[p_1,p_2,...,p_K]^{\mathrm{T}}$, and $\mathbf{i}=\mathrm{vec}(\mathbf{I})$. As defined in [21], the $\mathbf{A}_{\mathbb{D}}$ corresponds to steering matrix of the coarray, whose sensors are located at $\mathbb{D}d$, where

$$\mathbb{D}=\left\{l_m-l_n\,|m,n=0,1,...,2M+N-1\right\}. \tag{12}$$

Removing the repeated elements in $\mathbb{D}$, a subset $\mathbb{D}_u\subset\mathbb{D}$ with distinct elements is obtained, and then the difference coarray is defined as $\mathbb{D}_u d$. Accordingly, the virtual signals of the difference coarray is

$$\overline{\mathbf{x}}_{\mathbb{D}}=\overline{\mathbf{A}}_{\mathbb{D}}\mathbf{p}+\sigma_n^2\overline{\mathbf{i}}, \tag{13}$$

where $\overline{\mathbf{A}}_{\mathbb{D}}$ is the steering matrix of the difference coarray, $\overline{\mathbf{i}}$ is a sub-vector selected from the corresponding positions of $\mathbf{i}$.

As a property of the coprime array, there are "holes" in its difference coarray [22]. Namely, some elements are missing, leading to a non-uniform virtual array geometry. In order to apply the subspace based DOA estimation methods like MUSIC, which require for ULA, and make full use of all the received information, the matrix interpolation methods are developed to fill the holes. In such way, the missing correlation information of difference coarray is recovered; meanwhile the corresponding reconstructed virtual ULA is defined as $\mathbb{V}d$, where $\mathbb{V}$ is an integers set given by

$$\mathbb{V}=\left\{m\,|\,\min\left(\mathbb{D}\right)\le m\le\max\left(\mathbb{D}\right)\right\}. \tag{14}$$

The covariance matrix of the reconstructed virtual ULA, denoted as $\mathbf{R}_{\mathbb{V}}$, is a low-rank Hermitian Toeplitz matrix. Exploiting its structural property, the recovery of $\mathbf{R}_{\mathbb{V}}$ can be formulated as a nuclear norm minimization problem as follow:

$$\begin{aligned}\mathbf{R}_{\mathbb{V}}^{*}=&\arg\min_{\mathbf{R}_{\mathbb{V}}\in\mathbb{C}^{|\mathbb{V}^{+}|\times|\mathbb{V}^{+}|}}\left\|\mathbf{R}_{\mathbb{V}}\right\|_{*}\\ \text{s.t.}\quad&\mathbf{R}_{\mathbb{V}}=\mathbf{R}_{\mathbb{V}}^{\mathrm{H}}\\ &\left\langle\mathbf{R}_{\mathbb{V}}\right\rangle_{n_1,n_2}=\left\langle\overline{\mathbf{x}}_{\mathbb{D}}\right\rangle_{n_1-n_2}\end{aligned} \tag{15}$$

where $\|\cdot\|_{*}$ denotes the nuclear norm of a matrix, $\mathbb{V}^{+}=\left\{n\,|\,n\in\mathbb{V},n\ge 0\right\}$ is the non-negative part of $\mathbb{V}$. The second equality constraint holds true for all $\left\{n_1,n_2\,|\,n_1,n_2\in\mathbb{V}^{+},n_1-n_2\in\mathbb{D}\right\}$. The problem (15) can be efficiently solved by semidefinite programming since nuclear norm is a convex surrogate for matrix rank, and the optimal solution of this problem, $\mathbf{R}_{\mathbb{V}}^{*}$, can be directly used for MUSIC to estimate the DOAs. Besides, the DOF offered by the coprime array increases to $\left(|\mathbb{D}|-1\right)/2$ instead of $\left(|\mathbb{V}|-1\right)/2$.

B. MCC THEORY

Consider that the distorted observations appear in the nuclear norm minimization problem. Vectorizing the distorted covariance matrix $\hat{\mathbf{R}}_{\mathbb{S}}^{o}$, the affected virtual signal is given by

$$\mathbf{x}_{\mathbb{D}}^{o}=\mathrm{vec}\left(\hat{\mathbf{R}}_{\mathbb{S}}^{o}\right)=\mathbf{A}_{\mathbb{D}}^{o}\mathbf{p}+\sigma_n^2\mathbf{i}, \tag{16}$$

where $\mathbf{A}_{\mathbb{D}}^{o}=\left(\mathbf{\Gamma}\mathbf{A}\right)^{*}\odot\left(\mathbf{\Gamma}\mathbf{A}\right)$. Therefore, when there are some outlier observations, the second equality constraint in (15) becomes

$$\left\langle\mathbf{R}_{\mathbb{V}}\right\rangle_{n_1,n_2}=\left\langle\overline{\mathbf{x}}_{\mathbb{D}}^{o}\right\rangle_{n_1-n_2}. \tag{17}$$

Here, $\overline{\mathbf{x}}_{\mathbb{D}}^{o}$ is the virtual signal of the difference coarray distorted by the unknown matrix $\mathbf{\Gamma}$. In particular, since the equality constraint condition is based on the assumption that all the correlation information is correct, the equality constraint (17) tremendously amplifies the contribution of outlier samples due to miscalibration and thus yields large DOA estimation errors. To address this problem, the maximum correntropy criterion is introduced in this work to replace the equality constraint condition.

Correntropy is a generalized similarity measure between two random variables X and Y, defined by [23]

$$V_{\sigma}(X,Y)=\mathrm{E}[\kappa_{\sigma}(X-Y)], \tag{18}$$

where

$$\kappa_{\sigma}(X-Y)=\frac{1}{\sqrt{2\pi}\sigma}\exp\left(-\frac{(X-Y)^2}{2\sigma^2}\right) \tag{19}$$

is the Gaussian kernel function, σ is the kernel size. Usually, the kernel size σ is a user-selected free parameter which controls the observation window. In practice, the joint probability distribution function of the random variables is unknown and only a finite of samples $\left\{\left(x_i,y_i\right)\right\}_{i=1}^{N}$ are available, so the computation of correntropy is reformed as

$$\hat{V}_{N,\sigma}(X,Y)=\frac{1}{N}\sum_{i=1}^{N}\kappa_{\sigma}(x_i-y_i). \tag{20}$$

Since correntropy quantifies how different X is from Y in probability, it can be utilized as an error criterion for adaptive systems training. The larger correntropy indicates greater similarity between two random variables; therefore the maximum correntropy criterion is intuitively defined to ensure the fitting precision. Let $\boldsymbol{\theta}$ denote a set of adjustable parameters to be estimated and $\tilde{E}=X-Y$. Then the MCC is defined as

This article has been accepted for publication in a future issue of this journal, but has not been fully edited. Content may change prior to final publication. Citation information: DOI 10.1109/ACCESS.2020.2971842, IEEE Access

$$\begin{aligned}&\max_{\theta}\ \mathrm{E}\left[\kappa_\sigma\left(X-Y\right)\right]\\&=\max_{\theta}\ \iint_{x,y}\kappa_\sigma\left(x-y\right)f_{XY}(x,y)dxdy\,,\\&=\max_{\theta}\ \int_{\tilde{e}}\kappa_\sigma\left(\tilde{e}\right)f_{\tilde{E}}(x,y)d\tilde{e}\end{aligned}\tag{21}$$

In practice, the MCC is computed by its sample estimator:

$$\begin{aligned}&\max_{\theta}\ \frac{1}{N}\sum_{i=1}^{N}\kappa_\sigma\left(x_i-y_i\right)\\&=\max_{\theta}\ \frac{1}{N}\sum_{i=1}^{N}\kappa_\sigma\left(\tilde{e}_i\right)\end{aligned}\,.\tag{22}$$

Correntropy is a local similarity measure whose value is primarily dictated by the kernel function along the $x = y$ line, implying that the MCC is inherently insensitive to the outliers. Thus, the MCC outperforms the second equality constraint in (15) when some sensors are miscalibrated.

IV. PROPOSED METHOD

A. IMCC-NNM METHOD

As introduced above, the interpolation results acquired from NNM are distorted when some sensors in the array are miscalibrated, leading to inaccurate DOA estimation. In this subsection, the MCC is applied to develop a robust NNM based interpolation method, which is used to alleviate the influence of the outliers and thus provide reliable DOA estimation. At first, the definitions of selection matrix **S** and baseline matrix **B** are given below:

Definition 1. *The selection matrix* **S** *is a binary matrix of size* $\left|\mathbb{V}^+\right|\times\left|\mathbb{V}^+\right|$, *which distinguishes the known correlation information* (*elements set as one*) *and statistics to be interpolated* (*elements set as zero*), *i.e.*

$$\left[\mathbf{S}\right]_{i,j}=\begin{cases}1,\ \textit{if}\ \ i\in\mathbb{S}\ \textit{and}\ j\in\mathbb{S}\,,\\0,\ \textit{otherwise.}\end{cases}\tag{23}$$

Definition 2. *The baseline matrix* **B** *is a complex matrix of size* $\left|\mathbb{V}^+\right|\times\left|\mathbb{V}^+\right|$, *which contains all known correlation information at corresponding locations, while other elements are set as zero, i.e.*

$$\left\langle\mathbf{B}\right\rangle_{i,j}=\begin{cases}\left\langle\hat{\mathbf{R}}_{\mathbb{S}}^{o}\right\rangle_{i,j},\ \textit{if}\ \in\mathbb{S}\ \textit{and}\ j\in\mathbb{S},\\0,\ \textit{otherwise.}\end{cases}\tag{24}$$

Let $\tilde{\mathbf{E}}\in\mathbb{C}^{\left|\mathbb{V}^+\right|\times\left|\mathbb{V}^+\right|}$ be the residual error matrix, whose elements are then defined as

$$\left[\tilde{\mathbf{E}}\right]_{i,j}=\tilde{e}_{i,j}=\left|\left[\mathbf{R}_{\mathbb{V}}\circ\mathbf{S}\right]_{i,j}-\left[\mathbf{B}\right]_{i,j}\right|,\tag{25}$$

where $i=1,2,...,\left|\mathbb{V}^+\right|$ and $j=1,2,...,\left|\mathbb{V}^+\right|$. Therefore, we have

$$\sum_{i=1}^{\left|\mathbb{V}^+\right|}\sum_{j=1}^{\left|\mathbb{V}^+\right|}\tilde{e}_{i,j}^2=\sum_{i=1}^{\left|\mathbb{V}^+\right|}\sum_{j=1}^{\left|\mathbb{V}^+\right|}\left|\left[\mathbf{R}_{\mathbb{V}}\circ\mathbf{S}\right]_{i,j}-\left[\mathbf{B}\right]_{i,j}\right|^2.\tag{26}$$

With the definition of $\tilde{e}_{i,j}$, the MCC for the NNM problem is given in the form of sample estimator, as

$$\max_{\mathbf{R}_{\mathbb{V}}}\frac{1}{\left|\mathbb{V}^+\right|^2}\sum_{i=1}^{\left|\mathbb{V}^+\right|}\sum_{j=1}^{\left|\mathbb{V}^+\right|}\kappa_\sigma\left(\tilde{e}_{i,j}\right).\tag{27}$$

Since $\mathbf{R}_{\mathbb{V}}$ is a Hermitian Toeplitz matrix, all of the elements of this matrix can be defined by its first column. So, $\mathbf{R}_{\mathbb{V}}$ can be denoted as $\mathcal{T}(\mathbf{z})$, where $\mathbf{z}\in\mathbb{C}^{\left|\mathbb{V}^+\right|\times1}$ is the first column of $\mathbf{R}_{\mathbb{V}}$. With MCC, the NNM problem in (15) is reformulated in terms of Gaussian kernel function, expressed as

$$\begin{aligned}&\min_{\mathbf{z}}\left\|\mathcal{T}(\mathbf{z})\right\|_*\\&\text{s.t.}\ f_{\text{cons}}=\frac{1}{\left|\mathbb{V}^+\right|^2}\sum_{i=1}^{\left|\mathbb{V}^+\right|}\sum_{j=1}^{\left|\mathbb{V}^+\right|}\kappa_\sigma\left(\tilde{e}_{i,j}\right)>\varepsilon\end{aligned},\tag{28}$$

where $\varepsilon\in(0,1)$ is a user-specific threshold parameter to restrict the fitting error. The optimization problem (28) equals to

$$\begin{aligned}&\max_{\mathbf{z}}-\left\|\mathcal{T}(\mathbf{z})\right\|_*\\&\text{s.t.}\ f_{\text{cons}}=\frac{1}{\left|\mathbb{V}^+\right|^2}\sum_{i=1}^{\left|\mathbb{V}^+\right|}\sum_{j=1}^{\left|\mathbb{V}^+\right|}\kappa_\sigma\left(\tilde{e}_{i,j}\right)>\varepsilon\end{aligned}.\tag{29}$$

Then, it can be alternatively reformed as

$$\max_{\mathbf{z}}-\frac{1}{2}\left\|\mathcal{T}(\mathbf{z})\right\|_*+\frac{\tau}{\left|\mathbb{V}^+\right|^2}\sum_{i=1}^{\left|\mathbb{V}^+\right|}\sum_{j=1}^{\left|\mathbb{V}^+\right|}\kappa_\sigma\left(\tilde{e}_{i,j}\right),\tag{30}$$

where τ is a regularization parameter to balance the fitting error and the nuclear norm term.

However, the optimization problem (30) is difficult to solve because $\kappa_\sigma\left(\tilde{e}_{i,j}\right)$ is a nonlinear and nonconvex function. In order to efficiently solve this problem, the following proposition is introduced [22]:

Proposition 1. *For* $\kappa_\sigma\left(\tilde{e}\right)=\exp\left(-\left|\tilde{e}\right|^2/\left(2\sigma^2\right)\right)$, *there exists a convex conjugate function* Δ, *such that*

$$\kappa_\sigma\left(\tilde{e}\right)=\sup_{\omega}\left(\omega\frac{\left|\tilde{e}\right|^2}{2\sigma^2}-\Delta(\omega)\right),\tag{31}$$

and for a fixed $\tilde{e}$, *the supremum is reached at* $\omega=-\kappa_\sigma\left(\tilde{e}\right)$.

Utilizing the results of **Proposition 1**, the objective function (30) is converted to an augmented objective function in an enlarged parameter space,

$$\hat{F}\left(\mathbf{z},\mathbf{\Omega}\right)=\frac{\tau}{\left|\mathbb{V}^+\right|^2}\sum_{i=1}^{\left|\mathbb{V}^+\right|}\sum_{j=1}^{\left|\mathbb{V}^+\right|}\left(\omega_{i,j}\frac{\left|\tilde{e}_{i,j}\right|^2}{2\sigma^2}-\Delta\left(\omega_{i,j}\right)\right)-\frac{1}{2}\left\|\mathcal{T}(\mathbf{z})\right\|_*,\tag{32}$$

where $\mathbf{\Omega}$ is a $\left|\mathbb{V}^+\right|\times\left|\mathbb{V}^+\right|$ matrix storing the auxiliary variables with $\left[\mathbf{\Omega}\right]_{i,j}=\omega_{i,j}$. Denoting the original objective function (30) as $\hat{G}(\mathbf{z})$, according to **Proposition 1**, the following equation holds

$$\hat{G}(\mathbf{z})=\sup_{\mathbf{\Omega}}\hat{F}(\mathbf{z},\mathbf{\Omega}).\tag{33}$$

This article has been accepted for publication in a future issue of this journal, but has not been fully edited. Content may change prior to final publication. Citation information: DOI 10.1109/ACCESS.2020.2971842, IEEE Access

It follows that

$$\max_{\mathbf{z}} \hat{G}(\mathbf{z}) = \max_{\mathbf{z},\boldsymbol{\Omega}} \hat{F}(\mathbf{z},\boldsymbol{\Omega}), \tag{34}$$

which indicates that maximizing the augmented function $\hat{F}(\mathbf{z},\boldsymbol{\Omega})$ on the enlarged parameter space is equivalent to maximizing $\hat{G}(\mathbf{z})$. Exploiting the idea of alternate optimization approach, the value of augmented function in (34) can be maximized in an iterative way. Suppose that the local maximizer $(\mathbf{z},\boldsymbol{\Omega})$ at q-th iteration is obtained as $\mathbf{z}^{(q)}$ and $\boldsymbol{\Omega}^{(q)}$, the $\mathbf{z}^{(q+1)}$ and $\boldsymbol{\Omega}^{(q+1)}$ can be calculated in following way:

$$\omega_{i,j}^{(q+1)} = -\kappa_\sigma\left(\tilde{e}_{i,j}^{(q)}\right), \tag{35}$$

$$\mathbf{z}^{(q+1)} = \arg\max_{\mathbf{z}} \frac{\tau}{\left|\mathbb{V}^+\right|^2}\sum_{i=1}^{|\mathbb{V}^+|}\sum_{j=1}^{|\mathbb{V}^+|}\left(\omega_{i,j}^{(q+1)}\frac{\left|\tilde{e}_{i,j}\right|^2}{2\sigma^2} - \Delta(\omega_{i,j}^{(q+1)})\right) - \frac{1}{2}\left\|\mathcal{T}(\mathbf{z})\right\|_* . \tag{36}$$

Since the conjugate function $\Delta(\omega_{i,j})$ is a function of auxiliary parameter $\omega_{i,j}$ and is independent of $\mathbf{z}$ in each iteration, the optimization problem (36) can be simplified to

$$\mathbf{z}^{(q+1)} = \arg\max_{\mathbf{z}} \frac{\tau}{\left|\mathbb{V}^+\right|^2}\sum_{i=1}^{|\mathbb{V}^+|}\sum_{j=1}^{|\mathbb{V}^+|}\left(\omega_{i,j}^{(q+1)}\frac{\left|\tilde{e}_{i,j}\right|^2}{2\sigma^2}\right) - \frac{1}{2}\left\|\mathcal{T}(\mathbf{z})\right\|_* . \tag{37}$$

Obviously, the objective function in (37) is a concave function, so it can be solved efficiently by convex optimization method. The proposed iterative MCC embedded NNM interpolation method is referred to as IMCC-NNM, and for which, the following proposition is given:

Proposition 2. *Using IMCC-NNM, the objective function defined in (30) is not decreased and the iterative interpolation procedure is convergent.*

Proof: See Appendix A. ■

The relative error is used to examine the convergence. Specifically, the iterative process of IMCC-NNM is said to be converged if the following inequality holds

$$\left|\frac{\hat{F}^{(q)}(\mathbf{z},\boldsymbol{\Omega}) - \hat{F}^{(q-1)}(\mathbf{z},\boldsymbol{\Omega})}{\hat{F}^{(q-1)}(\mathbf{z},\boldsymbol{\Omega})}\right| \le \varepsilon_c \tag{38}$$

for some small tolerance ε_c. After the convergence of IMCC-NNM, the interpolation problem is solved, and thus the interpolated virtual ULA covariance matrix $\mathcal{T}(\hat{\mathbf{z}})$ is reconstructed with Hermitian Toeplitz structure. The proposed optimization problem can be viewed as a dual objective optimization problem; by solving which, the effect of outliers are eliminated the through the correntropy term, while the unknown entries in $\mathcal{T}(\hat{\mathbf{z}})$ are simultaneously recovered through the nuclear norm term. In addition, it is clear that, the absolute value of $\omega_{i,j} \in \{\omega_{i,j} \mid i \in \mathbb{S}, j \in \mathbb{S}\}$ is close to 1 if $[\mathcal{T}(\hat{\mathbf{z}})]_{i,j} \in \{[\mathcal{T}(\hat{\mathbf{z}})]_{i,j} \mid i \in \mathbb{S}, j \in \mathbb{S}\}$ corresponds to a calibrated sensor. Otherwise, absolute value of $\omega_{i,j} \in \{\omega_{i,j} \mid i \in \mathbb{S}, j \in \mathbb{S}\}$ should be close to 0 so as to suppress the effect of the miscalibrated outliers [18]. This intuitively explains how the proposed IMCC-NNM algorithm robustly reconstructs the covariance matrix $\mathbf{R}_{\mathbb{V}}$.

Because the robustly reconstructed $\mathcal{T}(\hat{\mathbf{z}})$ corresponds to a virtual ULA, whose achievable DOF is increased to $(|\mathbb{D}|-1)/2$, it can be directly utilized for the subspace based DOA estimation methods such as MUSIC. The MUSIC spatial spectrum can be computed as

$$\boldsymbol{f}_{\text{MUSIC}}(\theta) = \frac{1}{\mathbf{a}(\theta)^{\text{H}}\mathbf{N}_{\mathcal{T}(\hat{\mathbf{z}})}\mathbf{N}_{\mathcal{T}(\hat{\mathbf{z}})}^{\text{H}}\mathbf{a}(\theta)}, \tag{39}$$

where $\mathbf{N}_{\mathcal{T}(\hat{\mathbf{z}})}$ denotes the noise subspace, and it is obtained by collecting the eigenvectors corresponding to the $|\mathbb{V}^+|-K$ smallest eigenvalues. Finally, the DOAs can be estimated with higher credibility by searching the peaks of $\boldsymbol{f}_{\text{MUSIC}}(\theta)$.

The proposed robust DOA estimation algorithm for coprime array is summarized in **Algorithm 1** and has following key advantages. First, all available information received by the coprime array is effectively utilized for outlier suppression. Second, the objective function of optimization problem in each iteration is convex, which can be effectively solved by the well-developed interior point method. Third, the proposed method reconstructs the covariance matrix in a gridless manner, where the basis mismatch problem is avoided.

Algorithm 1: Robust DOA Estimation Algorithm for Coprime Array

1. Input: Coprime array received signals $\{\mathbf{x}(t)\}_{t=1}^{T}$.

2. Output: DOA Estimation $\hat{\theta}_k, k = 1,2,...,K$.

3. Initialization: Set the kernel size σ, $\hat{\mathbf{z}}^{(0)} = \mathbf{0}^{|\mathbb{V}^+|\times 1}$, maximum number of iteration Q, and index of iteration $q = 1$.

4. Compute $\hat{\mathbf{R}}_{\mathbb{S}}^{o}$ using equation (10);.

5. Define the selection matrix $\mathbf{S}$ by (23) and the baseline matrix $\mathbf{B}$ by (24);

6. Calculate $\omega_{i,j}^{(q)}$ using (25) and (35);

7. Solve (37) with $\omega_{i,j}^{(q)}$ to obtain $\hat{\mathbf{z}}^{(q)}$;

8. Let $q \leftarrow q+1$. Repeat Step 6 and Step 7 until convergence is achieved or q exceeds Q;

9. Calculate $\boldsymbol{f}_{\text{MUSIC}}(\theta)$ in (39) for DOA estimation.

B. COMPUTATIONAL COMPLEXITY

In this subsection, the computational complexity of the proposed IMCC-NNM algorithm is analyzed in terms of time complexity. The computational complexity for calculating the values of $\omega_{i,j}$ in each iteration is $\mathcal{O}\left(\left|\mathbb{V}^+\right|^2\right)$. The nuclear

norm of a matrix $\mathbf{Y}$ is defined as the sum of the singular values of this matrix, namely,

$$\|\mathbf{Y}\|_* = \tilde{\sigma}_1(\mathbf{Y}) + ... + \tilde{\sigma}_r(\mathbf{Y}) = \mathbf{tr}\left(\mathbf{Y}^{\mathrm{T}}\mathbf{Y}\right)^{1/2}, \quad (40)$$

where $\tilde{\sigma}_i(\mathbf{Y})$ $i = 1, 2..., r$ is the i-th largest singular value of $\mathbf{Y}$, and r is the rank of $\mathbf{Y}$. Therefore, the optimization problem in each iteration, as depicted in(37), can be viewed as quadratic programming problem. Utilizing the prime-dual interior point method to solve this problem, the computational complexity is $\mathcal{O}\left(\left|\mathbb{V}^+\right|\ln\left(1/\varepsilon_2\right)\right)$, where ε_2 is the convergence tolerance of the prime-dual interior point method. In a word, the computational complexity of the proposed algorithm can be roughly expressed as

$$\mathcal{O}\left(Q\left(\left|\mathbb{V}^+\right|^2 + \left|\mathbb{V}^+\right|\ln\left(1/\varepsilon_2\right)\right)\right). \quad (41)$$

C. CRAMÉR-RAO BOUND

Based on the stochastic Cramér-Rao Bound (CRB), which is the inverse of the Fisher information matrix (**FIM**), the DOA estimation performance of the proposed algorithm is analyzed. Since there is no additional information added during the interpolation procedure, the performance is determined by the physical coprime array. Thus, the **FIM** of the proposed algorithm is a function of the coprime array covariance matrix $\mathbf{R}_{\mathbb{S}}$, whose elements are expressed as

$$\left[\mathbf{FIM}\right]_{i,j} = T\mathbf{tr}\left(\mathbf{R}_{\mathbb{S}}^{-1}\frac{\partial\mathbf{R}_{\mathbb{S}}}{\partial\xi_i}\mathbf{R}_{\mathbb{S}}^{-1}\frac{\partial\mathbf{R}_{\mathbb{S}}}{\partial\xi_j}\right), \quad (42)$$

where ξ_i and ξ_j are the elements in the deterministic parameter vector $\boldsymbol{\xi}$.

However, when the coprime array is used to find more sources than sensors, the **FIM** defined in (42) is singular, which makes the CRB inapplicable. To address this issue, the vectorization process introduced in [25] is adopted, and the **FIM** is then transformed into a virtual array-based form as

$$\mathbf{FIM} = T\left[\mathrm{vec}\left(\frac{\partial\mathbf{R}_{\mathbb{S}}}{\partial\boldsymbol{\xi}^{\mathrm{T}}}\right)\right]^{\mathrm{H}}\left(\mathbf{R}_{\mathbb{S}}^{\mathrm{T}}\otimes\mathbf{R}_{\mathbb{S}}\right)^{-1}\left[\mathrm{vec}\left(\frac{\partial\mathbf{R}_{\mathbb{S}}}{\partial\boldsymbol{\xi}^{\mathrm{T}}}\right)\right], \quad (43)$$

which keeps nonsingular within a much broader range of conditions.

In this paper, the deterministic parameter vector is defined by

$$\boldsymbol{\xi} = \left[\boldsymbol{\theta}^{\mathrm{T}}, \boldsymbol{\rho}^{\mathrm{T}}, \boldsymbol{\phi}^{\mathrm{T}}, \mathbf{p}^{\mathrm{T}}, \sigma_n^2\right]^{\mathrm{T}}, \quad (44)$$

where $\boldsymbol{\rho} = \left[\rho_1, ..., \rho_{|\mathbb{S}|}\right]^{\mathrm{T}}$ and $\boldsymbol{\phi} = \left[\phi_1, ..., \phi_{|\mathbb{S}|}\right]$ are the gain distortion parameter vector and the phase distortion parameter vector respectively. Besides, denoting $\mathbf{P} = \mathrm{diag}(\boldsymbol{\rho})$ and $\boldsymbol{\Phi} = \mathrm{diag}(\boldsymbol{\phi})$, then the distortion parameter matrix $\boldsymbol{\Gamma}$ can be expressed as $\boldsymbol{\Gamma} = \mathbf{P}\boldsymbol{\Phi}$. Furthermore, the distorted manifold matrix $\mathbf{P}\boldsymbol{\Phi}\mathbf{A}$ is denoted as $\mathbf{P}\boldsymbol{\Phi}\mathbf{A} = \mathbf{H} = [\mathbf{h}_1, ..., \mathbf{h}_K]$ (i.e., $\mathbf{h}_i$ is the i-th column of $\mathbf{H}$), and the vector $\left[\mathbf{P}\boldsymbol{\Phi}\mathbf{A}\right]^* \odot \left[\mathbf{P}\boldsymbol{\Phi}\mathbf{A}\right]\mathbf{p}$ is denoted as $\left[\mathbf{P}\boldsymbol{\Phi}\mathbf{A}\right]^* \odot \left[\mathbf{P}\boldsymbol{\Phi}\mathbf{A}\right]\mathbf{p} = \left[c_1, ..., c_{|\mathbb{S}|^2}\right]^{\mathrm{T}}$. Accordingly, the **FIM** can be specified as

$$\mathbf{FIM} = T\left[\frac{\partial\mathbf{x}_{\mathbb{S}}^o}{\partial\boldsymbol{\xi}^{\mathrm{T}}}\right]^{\mathrm{H}}\left(\mathbf{R}_{\mathbb{S}}^{\mathrm{T}}\otimes\mathbf{R}_{\mathbb{S}}\right)^{-1}\left[\frac{\partial\mathbf{x}_{\mathbb{S}}^o}{\partial\boldsymbol{\xi}^{\mathrm{T}}}\right], \quad (45)$$

where

$$\begin{aligned}
&\frac{\partial\mathbf{x}_{\mathbb{S}}^o}{\partial\boldsymbol{\xi}^{\mathrm{T}}} = \left[\boldsymbol{\Lambda}_\theta \vdots \boldsymbol{\Lambda}_\rho \vdots \boldsymbol{\Lambda}_\phi \vdots \boldsymbol{\Lambda}_p \vdots \boldsymbol{\Lambda}_{\sigma_n^2}\right],\\
&\boldsymbol{\Lambda}_\theta = \left[\frac{\partial\mathbf{x}_{\mathbb{S}}^o}{\partial\theta_1}, ..., \frac{\partial\mathbf{x}_{\mathbb{S}}^o}{\partial\theta_K}\right],\\
&\boldsymbol{\Lambda}_p = \left[\frac{\partial\mathbf{x}_{\mathbb{S}}^o}{\partial p_1}, ..., \frac{\partial\mathbf{x}_{\mathbb{S}}^o}{\partial p_K}\right],\\
&\boldsymbol{\Lambda}_{\sigma_n^2} = \left[\frac{\partial\mathbf{x}_{\mathbb{S}}^o}{\partial\sigma_n^2}\right]
\end{aligned} \quad (46)$$

with

$$\begin{aligned}
&\boldsymbol{\Lambda}_\rho = \left[\left[\frac{\partial c_1}{\partial\boldsymbol{\rho}^{\mathrm{T}}}\right]^{\mathrm{T}}, ..., \left[\frac{\partial c_{(2M+N-1)^2}}{\partial\boldsymbol{\rho}^{\mathrm{T}}}\right]^{\mathrm{T}}\right]^{\mathrm{T}},\\
&\boldsymbol{\Lambda}_\phi = \left[\left[\frac{\partial c_1}{\partial\boldsymbol{\phi}^{\mathrm{T}}}\right]^{\mathrm{T}}, ..., \left[\frac{\partial c_{|\mathbb{S}|^2}}{\partial\boldsymbol{\phi}^{\mathrm{T}}}\right]^{\mathrm{T}}\right]^{\mathrm{T}},\\
&\frac{\partial\mathbf{x}_{\mathbb{S}}^o}{\partial\theta_k} = p_k\left[\frac{\partial\mathbf{h}_k^*}{\partial\theta_k}\otimes\mathbf{h}_k + \mathbf{h}_k^*\otimes\frac{\partial\mathbf{h}_k}{\partial\theta_k}\right],\\
&\frac{\partial\mathbf{x}_{\mathbb{S}}^o}{\partial p_k} = \mathbf{h}_k^*\otimes\mathbf{h}_k,\\
&\frac{\partial\mathbf{x}_{\mathbb{S}}^o}{\partial\sigma_n^2} = \mathbf{i}
\end{aligned} \quad (47)$$

Therefore, the CRB for the k-th source can be obtained as

$$\mathrm{CRB}\left(\theta_k\right) = \left[\mathbf{FIM}^{-1}\right]_{k,k} \quad (48)$$

for $1 \le k \le K$.

V. SIMULATION

In order to validate the robustness of the proposed algorithm, a series of computer simulations were performed. In these simulations, the pair of coprime integers $M = 3$ and $N = 5$ is chosen to deploy the coprime array, which yields an array with $|\mathbb{S}| = 2M + N - 1 = 10$ physical sensors located at $\{0, 3d, 5d, 6d, 9d, 10d, 12d, 15d, 20d, 25d\}$. Assume that $K = 11$ equal-power sources uniformly distributed in $\left[-50.2^\circ, 72.8^\circ\right]$ impinge on the array. For IMCC-NNM, the kernel size σ is chosen as 10, the regularization parameter τ is set as 0.5, the tolerance parameter ε_c is set as 10^{-5}, and the maximum iteration Q is selected as 50 empirically. The optimization problems are solved using the CVX [26].

In the first example, the convergence of IMCC-NNM is examined under different signal-to-noise ratios (SNRs). The

This article has been accepted for publication in a future issue of this journal, but has not been fully edited. Content may change prior to final publication. Citation information: DOI 10.1109/ACCESS.2020.2971842, IEEE Access

outliers are arbitrarily assumed to appear in the fourth and the eighth rows of the received signal vector $\{\mathbf{x}(t)\}_{t=1}^{T}$, i.e. $\mathbb{M}=\{4,8\}$. The specific values of the complex gain and phase distortions of the miscalibrated sensors are $3\exp(j4)$ and $4\exp(j3)$ respectively. It should be noted that both the positions and the distortions are unknown *a priori* for the tested algorithm. The number of snapshot is fixed at T = 1000 when the SNR varies.

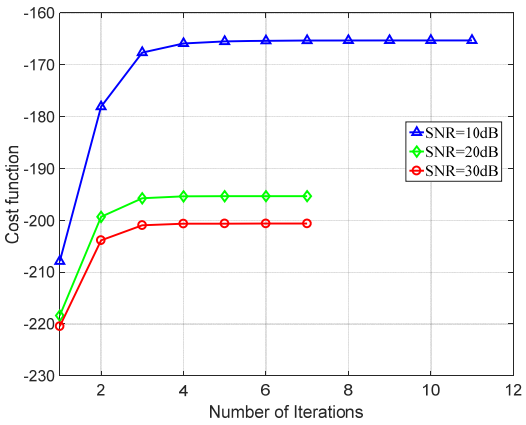

FIGURE 2. Convergence of IMCC-NNM algorithm under different SNR environments.

Using the settings defined above, Fig. 2 plots the convergence behaviors of IMCC-NNM algorithm at SNR = 10dB, 20dB and 30dB. Fig. 2 shows that, in the iteration process, the value of objective function remains non-decreasing for different SNR, and under such environments, the IMCC-NNM algorithm will converge within fifteen iterations. It can be also found that, the IMCC-NNM always converges to a smaller objective function value with higher SNR.

In following simulations, the proposed robust DOA estimation algorithm is compared to two non-robust DOA estimation algorithms utilizing coprime arrays, namely, the Spatial Smooth MUSIC algorithm (SS-MUSIC) [27] and the Nuclear Norm Minimization (NNM) algorithm [6]; it is also compared to three CS based robust DOA estimation algorithms, i.e., the Sparse Bayesian learning Array Calibration with physical array received signals (SBAC-1) algorithm [16], the Sparse Bayesian learning Array Calibration with second order virtual signals (SBAC-2) algorithm [17] and the Maximum Correntropy Criterion incorporated Compressive Sensing (CS-MCC) algorithm [18]. For the sake of computational complexity, the sampling interval of the pre-defined sampling grids is set as 0.5° for the SBAC-1 algorithm, the SBAC-2 algorithm and the CS-MCC algorithm. The tolerance parameter ε_c and the maximum iteration Q of the SBAC-1 algorithm, the SBAC - 2 algorithm and the CS-MCC algorithm are set the same as that of the IMCC-NNM algorithm. The kernel size of the CS-MCC algorithm is calculated using the Silverman's rule [23, 28].

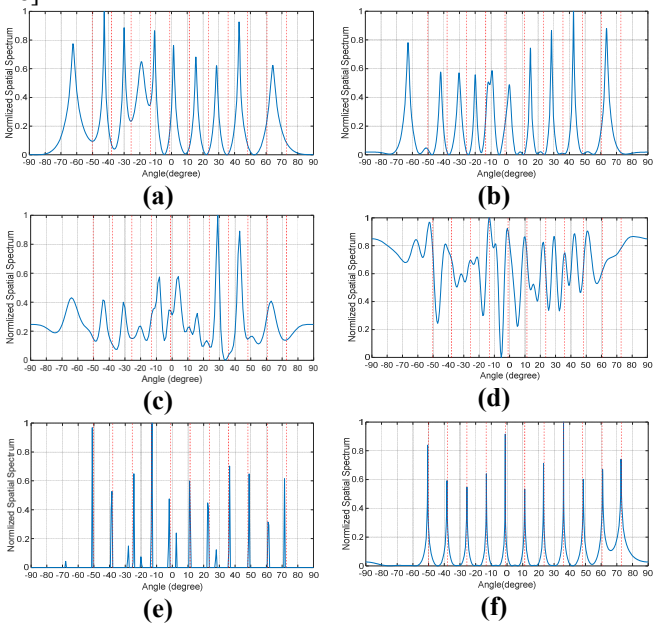

FIGURE 3. Accuracy comparison of DOA estimation in terms of the normalized spatial spectrum with SNR = 30dB and the number of snapshots T = 1000. (a) SS-MUSIC algorithm. (b) NNM algorithm. (c) SBAC-1 algorithm. (d) SBAC-2 algorithm. (e) CS-MCC algorithm. (f) IMCC-NNM algorithm.

In the second example, the DOA estimation accuracy of each algorithm in the presence of miscalibrated sensors is compared. Both the locations and the distortion parameters of the miscalibrated sensors are the same as in example 1. The SNRs of the sources are assumed to be 30dB, and the number of snapshots is selected as 1000. Fig. 3 depicts normalized spatial spectra estimated by all the algorithms, where the vertical dashed lines denote the actual directions of the incident sources. It is observed from Fig. 3(a) and Fig. 3(b) that the two non-robust DOA estimation algorithms (i.e. SS-MUSIC and NNM) cannot correctly resolve all the sources, while their estimation results deviate from the actual source directions. As shown in Fig. 3(c) and Fig. 3(d), both the SBAC-1 algorithm and SBAC-2 fail to calibrate the gain and phase distortions in such a case. The number of peaks in the spatial spectrum of the SBAC-1 algorithm is less than the sources number K, while the number of peaks in the spatial spectrum of the SBAC-2 algorithm is more than the sources number K. At the same time, very few of their peaks are closed to corresponding positions of the actual source directions. Fig. 3(d) shows that although there are some low pseudo-peaks in its the spatial spectrum, the CS-MCC algorithm correctly resolved the sources. However, there are still some deviations in the estimation results of the CS-MCC algorithm duo to the grid mismatch. In contrast, the proposed IMCC-NNM algorithm shows better estimation accuracy in Fig. 3(e) since it is a gridless algorithm.

This article has been accepted for publication in a future issue of this journal, but has not been fully edited. Content may change prior to final publication. Citation information: DOI 10.1109/ACCESS.2020.2971842, IEEE Access

In the third example, the root mean square error (RMSE) of each algorithm is compared in Fig. 4. Here, the RMSE is defined as

$$\mathrm{RMSE}=\sqrt{\frac{1}{KQ_M}\sum_{k=1}^{K}\sum_{q_M=1}^{Q_M}\left(\hat{\theta}_k\left(q_M\right)-\theta_k\right)}, \tag{49}$$

where $\hat{\theta}_k\left(q_M\right)$ is the estimated DOA of the k-th source in the q_M-th Monte Carlo trial, Q_M is the number of Monte Carlo trials. It can be seen from example 2 that, under some conditions, some of algorithms cannot correctly distinguish the number of source. Therefore, for statistical convenience, the number of sources K is considered as known, and the angels corresponding to K highest peaks in spatial spectra are picked as estimated DOAs. The number of snapshots is fixed at $T = 2000$ when the SNR varies, whereas the SNR is fixed at 30 dB when the number of snapshots varies. The locations and the distortion parameters of the miscalibrated sensors are also set the same as in example 1. For each data point, $Q_M = 500$ Monte Carlo trials are conducted to calculate the RMSE. The Cramér-Rao bound (CRB) (48) is also plotted

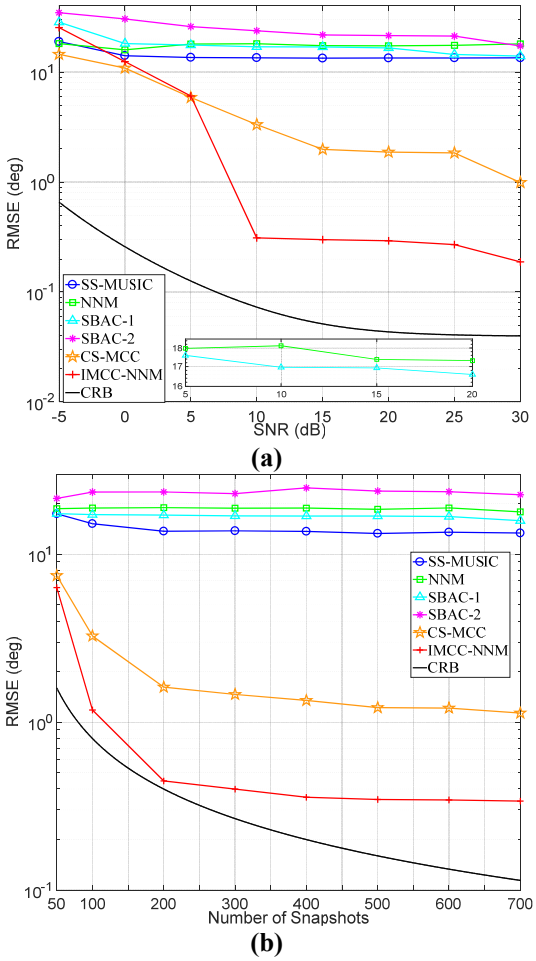

FIGURE 4. RMSE performance comparison with 11 incident sources. (a) RMSE versus SNR with the number of snapshots T = 2000. (b) RMSE versus the number of snapshots with SNR = 30dB.

It can be seen in Fig. 4(a) that with the increase of SNR, there is no obvious change in the DOA estimation RMSE of the SS-MUSIC algorithm and the NNM algorithm because DOA estimation deviation of these algorithms is mainly cause by the outliers, and increasing SNR will not reduce the influence of outliers. Comparing with these two non-robust DOA estimation algorithms, the SBAC-1 algorithm does not show obvious calibration effect and the SBAC-2 algorithm shows even worse RMSE performance under such serious disturbance. The CS-MCC algorithm and the IMCC-NNM algorithm do not show better DOA estimation accuracy when the SNR is lower than 0dB. Nevertheless, it is demonstrated in Fig. 4(a) that the CS-MCC algorithm and the proposed algorithm can effectively mitigate the influence of the outliers when the SNR is higher than 5 dB. It is because that the difference between the outliers and the normal signals is not significant for MCC to distinguish the outlier when the SNR is lower than 0 dB. Besides, the RMSE of the IMCC-NNM algorithm is smaller than that of the CS-MCC algorithm when the SNR is higher than 10 dB. The reason lies in that the sampling grids defined by the fixed sampling interval lead to a basis mismatch, limiting the estimation accuracy of the CS-MCC algorithm. Similar performance comparison can also be found in Fig. 4(b), where the number of snapshots is varied. As shown in Fig. 4(b), the RMSEs of the CS-MCC algorithm and the proposed algorithm are smaller than that of other algorithms even when the number of snapshot is small. Moreover, the RMSE of the IMCC-NNM algorithm is significantly smaller than that of the CS-MCC when the number of snapshots is larger than 50.

In the fourth example, both the DOA estimation accuracy and the robustness of the tested algorithms are compared in the presence of miscalibrated sensors. Here the deviation distance of estimation (DDOE) of the q_M-th Monte Carlo trial is defined as

$$\mathrm{DDOE}^{(q_M)}=\sqrt{\sum_{k=1}^{K}\left(\hat{\theta}_k(q_M)-\theta_k\right)}. \tag{50}$$

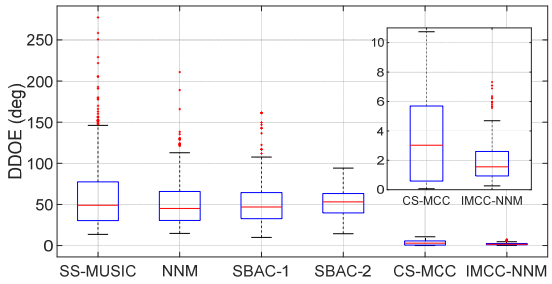

FIGURE 5. Box plots of DDOE for the tested algorithms when the distortion parameters are fixed and the locations of the miscalibrated sensors are randomly selected.

This article has been accepted for publication in a future issue of this journal, but has not been fully edited. Content may change prior to final publication. Citation information: DOI 10.1109/ACCESS.2020.2971842, IEEE Access

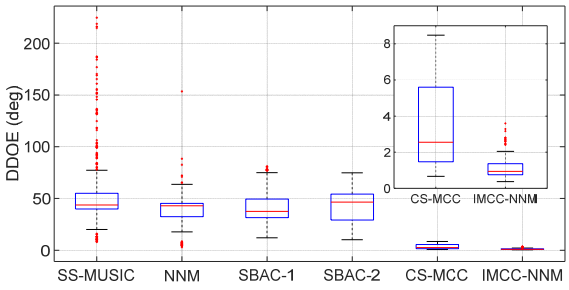

FIGURE 6. Box plots of DDOE for the tested algorithms when the locations of the miscalibrated sensors are fixed and the distortion parameters are randomly selected.

For the same reason as stated in example 2, the number of sources K is considered as known. The SNR and the number of snapshot in this example are set as 30dB and 2000 respectively. Assume that there are two miscalibrated sensors in the array, whose locations are randomly selected among $\mathbb{L}$ in each Monte Carlo trial, while specific values of the distortion parameters of the them are fixed at $3\exp(j4)$ and $4\exp(j3)$ respectively. Box plots of DDOE of the testing algorithms are shown in Fig. 5, where the statistical data is collected from 500 Monte Carlo trials for each algorithm. As can be seen from Fig. 5, the average value of the DDOEs obtained by the proposed IMCC-NNM algorithm is the smallest, and the box of IMCC-NNM has the lowest height with fewest outliers. Thus, the IMCC-NNM algorithm outperforms other algorithms in terms of both estimation accuracy and robustness in the presence of miscalibrated sensors. In turn, assume that the sensor miscalibrations occur fixedly on the fourth and eighth sensors in the array, i.e., $\mathbb{M}=\{4,8\}$, while the gain distortion parameters $\{\rho_m\}_{m=1}^2$ are randomly chosen from the interval [2,4] and the phase distortion parameters $\{\phi_m\}_{m=1}^2$ are randomly chosen from the interval [1,3]. The box plots of DDOE of the testing algorithms shown in Fig. 6 also verify the superiority of the proposed algorithm.

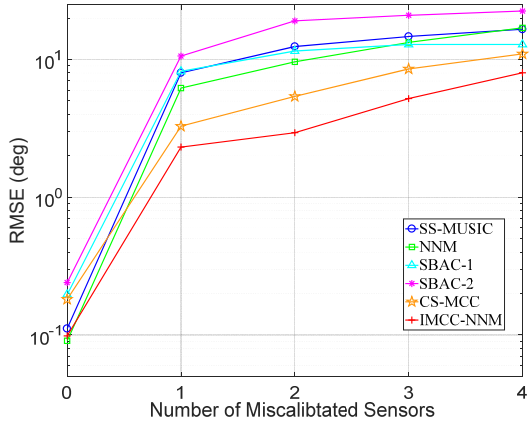

FIGURE 7. RMSE performance comparison with different number of miscalibrated sensors.

In the fifth example, the RMSE performance is compared with respect to the number of miscalibrated sensors in the case of SNR = 30dB and T = 2000. Since the proposed IMCC-NNM treats the information received by the miscalibrated sensors as outliers, the number of miscalibrated sensors is assumed to be less than fifty percent of the total number of sensors, i.e. the number of miscalibrated sensors is assumed to be less than 5. At each number of miscalibrated sensors, the locations of the miscalibrated sensors are randomly selected from $\mathbb{L}$, the gain distortion parameters ρ_m are randomly chosen from the interval [2,3] and the phase distortion parameters ϕ_m are randomly chosen from the interval [1,2]. For each data point, the RMSE is calculated from Q = 500 Monte Carlo trials. According to the comparison results shown in Fig. 7, when there is no miscalibrated sensor, the RMSE of IMCC-NNM is equivalent to those of the other subspace based DOA estimation algorithms (i.e. the SS-MUSIC algorithm and NNM algorithm); meanwhile the SBAC-2 algorithm has the largest RMSE in such a case. When the number of miscalibrated sensors varies from 1 to 4, the IMCC-NNM always has the smallest RMSE, but the estimation accuracy advantage of IMCC-NNM is reduced as the number of miscalibrated sensors is increased to 4. Therefore, Fig. 7 demonstrates the better overall performance of IMCC-NNM over other DOA algorithms when there are miscalibrated sensors in the coprime array.

VI. CONCLUSIONS

In this paper, we address the problem of estimating DOA using a coprime array with miscalibrated sensors. A novel robust virtual array interpolation method, referred as to IMCC-NNM, was proposed to generate a virtual ULA while alleviate the influence of miscalibrated sensors, where all information of the coprime array received signals is included. Without *a priori* knowledge of the miscalibrated sensors, the information received by them is implicitly treated as outliers, and the correntropy is introduced as the robust similarity measurement. An optimization problem is formulated as minimizing the nuclear norm of a covariance matrix of the virtual signal under the maximum correntropy criterion in a gridless manner. To solve the optimization problem, an iterative convex optimization algorithm was developed and the convergence of this algorithm was proved. Utilizing the reconstructed Toeplitz covariance matrix, a more credible DOA estimation can be obtained with an increased number of DOFs. The robustness of the proposed algorithm is clearly verified through simulation comparisons with existing algorithms using coprime arrays.

Appendix A
PROOF OF PROPOSITION 2

The difference between the results of any two adjacent iterations can be calculated as

$$\hat{F}^{(q)}-\hat{F}^{(q-1)}=\left[\hat{F}\left(\mathbf{z}^{(q)},\boldsymbol{\Omega}^{(q)}\right)-\hat{F}\left(\mathbf{z}^{(q-1)},\boldsymbol{\Omega}^{(q)}\right)\right]+\left[\hat{F}\left(\mathbf{z}^{(q-1)},\boldsymbol{\Omega}^{(q)}\right)-\hat{F}\left(\mathbf{z}^{(q-1)},\boldsymbol{\Omega}^{(q-1)}\right)\right]. \quad (51)$$

Because the q-th iteration results $\mathbf{z}^{(q)}$ and $\boldsymbol{\Omega}^{(q)}$ are obtained by solving the maximum problem of (31) and (32), the following inequalities hold true

$$\hat{F}\left(\mathbf{z}^{(q)},\boldsymbol{\Omega}^{(q)}\right)\geq\hat{F}\left(\mathbf{z}^{(q-1)},\boldsymbol{\Omega}^{(q)}\right)\geq\hat{F}\left(\mathbf{z}^{(q-1)},\boldsymbol{\Omega}^{(q-1)}\right) \quad (52)$$

Therefore, $\hat{F}^{(q)}-\hat{F}^{(q-1)}\geq 0$ and then the sequence $\left\{\hat{F}^{(q)}\right\}_{q=1,2,\ldots}$ is non-decreasing. In addition, both the correntropy and the nuclear norm term in (32) are upper bounded, i.e.,

$$0\leq\kappa_{\sigma}\left(e_{i,j}\right)\leq\frac{1}{\sqrt{2\pi}\sigma},\qquad -\left\|\mathcal{T}\left(\mathbf{z}\right)\right\|_{*}\leq 0. \quad (53)$$

Consequently, it can be concluded that the proposed IMCC-NNM algorithm is convergent. ■

REFERENCES

[1] H. Krim and M. Viberg, "Two decades of array signal processing research - The parametric approach," *IEEE Signal Process. Mag*., vol. 13, no. 4, pp. 67-94, Jul 1996.

[2] H.L.V. Trees, *Detection, Estimation, and Modulation Theory, Part IV: Optimum Array Processing*. New York, NY, USA: Wiley, 2004.

[3] T.E. Tuncer and B. Friedlander, "Practical Aspects of Design and Application of Direction-Finding Systems," in *Classical and Modern Direction-of-Arrival Estimation*, USA: Academic Press. 2009.

[4] P. Stoica and A. Nehorai, "MUSIC, maximum-likelihood, and Cramér-Rao bound," *IEEE Trans. Acoust., Speech, Signal Process.*, vol. 37, no. 5, pp. 720-741, May 1989.

[5] M.E. Davies and Y.C. Eldar, "Rank awareness in joint sparse recovery," *IEEE Trans. Inf. Theory.*, vol. 58, no.2, pp.1135-1146, Feb. 2012.

[6] C.L. Liu, P.P. Vaidyanathan and P. Pal, "Coprime coarray interpolation for DOA estimation via nuclear norm minimization," in *Proc. of the 2016 IEEE Int. Symp. Circuits and Syst.*, Montréal, QC, Canada, May 2016, pp. 2639-2642.

[7] C.L. Liu and P.P. Vaidyanathan, "Remarks on the spatial smoothing step in coarray MUSIC," *IEEE Signal Process. Lett.* Vol. 22, no. 9, pp. 1438-1442, Feb. 2015.

[8] M.R. Guo, T. Chen and B. Wang, "An improved DOA estimation approach using coarray interpolation and matrix denoising," *Sensors*, vol. 17, no. 5, pp. 1-12, May 2017

[9] Y.I. Abramovich, N.K. Spencer and A.Y. Gorokhov, "Positive-definite Toeplitz completion in DOA estimation for nonuniform linear antenna arrays - part II: Partially augmentable arrays," *IEEE Trans. Signal Process.*, vol. 47, no. 6, pp. 1502-1521, Jun. 1999.

[10] C.W. Zhou, Y.J. Gu, X. Fan, Z.G. Shi, G.Q. Mao and Y.M.D. Zhang, "Direction-of-arrival estimation for coprime array via virtual array interpolation," *IEEE Trans. Signal Process.,* vol. 66, no. 22, pp. 5956-5971, Nov 2018.

[11] C.W. Zhou, Y.J. Gu, Z.G. Shi and Y.M.D. Zhang, "Off-grid direction-of-arrival estimation using coprime array interpolation," *IEEE Signal Process. Lett.,* vol. 25, no. 11, pp. 1710-1714, Nov 2018.

[12] M. Wang, Z. Zhang and A. Nehorai, "Performance analysis of coarray-based MUSIC in the presence of sensor location errors," *IEEE Trans. Signal Process*., vol. 66, no. 12, pp. 3074-3085, Jun. 2018.

[13] A.J. Weiss and B. Friedlander, "Eigenstructure methods for direction finding with sensor gain and phase uncertainties," *Circuits Syst. Signal Process.*, vol. 9, no. 3, pp. 271-300, Sep. 1990.

[14] A.F. Liu, G.S. Liao, C. Zeng, Z.W. Yang, and Q. Xu, "An eigenstructure method for estimating DOA and sensor gain-phase errors," *IEEE Trans. on Signal Process.*, vol. 59, no. 12, pp. 5944-5956, Aug. 2011.

[15] A.F. Liu and G.S. Liao, "An eigenvector based method for estimating DOA and sensor gain-phase errors," *Digit. Signal Process.*, vol. 79, pp. 116-124, Aug. 2018.

[16] Z.M. Liu and Y.Y. Zhou, "A unified framework and sparse Bayesian perspective for direction-of-arrival estimation in the presence of array imperfections," *IEEE Trans. Signal Process.,* vol. 61, no. 15, pp. 3786-3798, Aug 2013.

[17] R. Lu, M. Zhang, X.B. Liu, X.M. Chen and A.X .Zhang, "Direction-of-arrival estimation via coarray with model errors," *IEEE Access*, vol. 6, pp. 54514-54525, Oct. 2018.

[18] B. Wang, Y.M.D. Zhang and W. Wang, "Robust DOA estimation in the presence of miscalibrated sensors," *IEEE Signal Process. Lett.*, vol. 24, no. 7, pp. 1073-1077, Jul. 2017.

[19] J.X. Kou, M. Li, and C.L. Jiang, "A Robust DOA Estimator Based on Compressive Sensing for Coprime Array in the Presence of Miscalibrated Sensors," *Sensors*, vol. 19, no. 16, pp. 1-17, Aug 2019.

[20] N.R. Goodman, "Statistical-analysis based on a certain multivariate complex Gaussian distribution (an introduction)," *Ann. Stat.*, vol. 34, no.1, pp. 152-177, Mar. 1963.

[21] P. Pal and P.P Vaidyanathan, "Nested Arrays: A novel approach to array processing with enhanced degrees of freedom," *IEEE Trans. Signal Process.*, vol. 58, no. , pp. 4167-4181, Aug. 2010.

[22] P.P. Vaidyanathan and P. Pal, "Sparse sensing with co-prime samplers and arrays," *IEEE Trans. Signal Process.* vol. 59, no. 2, pp. 573- 586, Feb. 2011.

[23] W. Liu, P.P. Pokharel and Principe J.C., "Correntropy: properties and applications in non-Gaussian signal processing," *IEEE Trans. Signal Process.*, vol. 55, no. 11, pp. 5286-5298, Nov. 2007.

[24] X. Yuan, B.G. Hu, "Robust feature extraction via information theoretic learning," in *Proc. Int. Conf. Mach. Learn.*, Montréal, QC, Canada, June 2009, pp. 1193–1200.

[25] C.L. Liu and P.P. Vaidyanathan, "Cramér-Rao bounds for coprime and other sparse arrays, which find more sources than sensors," *Digit. Signal Prog.*, vol. 61, pp. 43-61, Feb. 2017.

[26] M. Grant, and S. Boyd, CVX: "Matlab software for disciplined convex programming, version 2.1," Mar. 2014, [Online] Available: http://cvxr.com/cvx

[27] P. Pal and P.P. Vaidyanathan, "Coprime sampling and the MUSIC algorithm," in *Proc. the IEEE Digit. Signal Process. Workshop / IEEE Signal Process. Educ. Workshop*, Sedona, AZ, USA, January 2011; pp. 289–294.

[28] J.L. Liang, D. Wang, L. Su B.D. Chen, H. Chen and H.C. So, "Robust MIMO radar target localization via nonconvex optimization," *Signal Process.*, vol. 122, pp. 33-38, May 2016.

JIAXUN KOU was born in Chengdu, China, in 1989. He received the B.Eng. degree in armored vehicle engineering from the North University of China, Taiyuan, China, in 2012, the M.Sc. degree in aeronautical and astronautical science and technology from Beijing Institute of Technology, Beijing, China, in 2016. He is currently pursuing the Ph.D. degree with School of Mechatronical Engineering, Beijing Institute of Technology, China. His research interests include array signal processing, direction-of-arrival estimation and their applications in intelligent munitions system.

MING LI received the B.Eng. and M.Sc. degrees in ammunition engineering and the Ph.D. degree in mechatronic engineering from Beijing Institute of Technology, Beijing, China, in 1998, 2001, and 2004, respectively.

He is currently an Associate Professor with School of Mechatronical Engineering, Beijing Institute of Technology. His research interests include array signal processing, wireless sensor network technology, hardware technology of digital signal processing and their applications in intelligent munitions system.

CHUNLAN JIANG received the B.Eng. in ammunition engineering, the M.Sc. degree in explosion mechanics and the Ph.D. degree in artillery, automatic weapons and ammunition engineering from Beijing Institute of Technology, Beijing, China, in 1983, 1986, and 2002, respectively.

From 1995 to 1996, she was a Visiting Researcher with The University of Sydney, Australia. Since 2000, she has been a Professor with the School Mechatronical Engineering, Beijing Institute of Technology. Her research interests are in the general area of ammunition engineering

Dr. Jiang was a recipient of the First Prize of National Defense Technology Invention Award in 2013 and Second Prize of National Technical Invention Award in 2015.